Two electric field Monte Carlo models of coherent backscattering of polarized light

Alexander Doronin,[1] Andrew J. Radosevich,[2] Vadim Backman,[2] and Igor Meglinski[1,*]

[1]*Jack Dodd Center for Quantum Technologies, Department of Physics, University of Otago, P.O. Box 56, Dunedin 9054, New Zealand*

[2]*Department of Biomedical Engineering, Northwestern University, Tech E310, 2145 Sheridan Road, Evanston, Illinois, USA*

**Corresponding author: igor.meglinski@otago.ac.nz*

Received May 30, 2014; revised September 17, 2014; accepted September 17, 2014; posted September 17, 2014 (Doc. ID 212817); published October 14, 2014

Modeling of coherent polarized light propagation in turbid scattering medium by the Monte Carlo method provides an ultimate understanding of coherent effects of multiple scattering, such as enhancement of coherent backscattering and peculiarities of laser speckle formation in dynamic light scattering (DLS) and optical coherence tomography (OCT) diagnostic modalities. In this report, we consider two major ways of modeling the coherent polarized light propagation in scattering tissue-like turbid media. The first approach is based on tracking transformations of the electric field along the ray propagation. The second one is developed in analogy to the iterative procedure of the solution of the Bethe–Salpeter equation. To achieve a higher accuracy in the results and to speed up the modeling, both codes utilize the implementation of parallel computing on NVIDIA Graphics Processing Units (GPUs) with Compute Unified Device Architecture (CUDA). We compare these two approaches through simulations of the enhancement of coherent backscattering of polarized light and evaluate the accuracy of each technique with the results of a known analytical solution. The advantages and disadvantages of each computational approach and their further developments are discussed. Both codes are available online and are ready for immediate use or download.

OCIS codes: (070.7345) Wave propagation; (170.3660) Light propagation in tissues; (260.5430) Polarization; (290.1350) Backscattering; (290.5855) Scattering, polarization.

http://dx.doi.org/10.1364/JOSAA.31.002394

1. INTRODUCTION

Studying the propagation of coherent polarized light in turbid tissue-like scattering media is a fascinating topic of research that provides an understanding of the coherent effects of multiple scattering, such as an enhancement of coherent backscattering (EBS) and formation of laser speckles in optical coherence tomography (OCT) and in dynamic light scattering (DLS). Because of the diversity of probing conditions for complex composite materials, including biological tissues, there is no analytical solution that can fully describe the transfer of coherent polarized light in such turbid tissue-like media. Stochastic techniques such as Monte Carlo (MC) modeling provide a solution to the radiative transfer equation for cases where an analytical solution is impossible to obtain. Therefore, nowadays MC has become the "gold standard" technique for studying light propagation and scattering in complex media, and more than 1,000 MC-based codes have been developed for various diagnostic applications. A number of MC codes have been specially developed to track the state of polarization of light propagating through a scattering medium. Utilizing the Stokes–Mueller formalism, the propagation of incoherent polarized light in turbid media has been described by Kattawar and Plass [1], Bartel and Hielscher [2], Wang and Wang [3], Côté and Vitkin [4], Ramella-Roman *et al.* [5], and others. Still, these codes are not fully capable of describing the complexities of spatially and temporally coherent light, including effects of multiple scattering, such as EBS [6–9].

Enhancement of coherent backscattering, known also as coherent backscattering (CBS), is a coherent wave phenomenon in which light rays traveling through time-reversed paths (i.e., two light rays that travel through the same sequence of optical events but in the opposite directions relative to each other) interfere constructively to create an angular intensity peak centered around the backscattering direction. A single time-reversed path can be thought of as one Young's double pinhole experiment, where the separation between the two pinholes is determined by the exit positions of the time-reversed rays [Fig. 1(a)]. The spherical waves emanating from these two points form a cosine angular diffraction pattern in the far field [Fig. 1(b) and Media 1].

In other words, the diffraction pattern is simply the 2D Fourier transform of the spatial pinhole distribution. In a tissue-like medium where light is multiply scattered, there are an infinite number of time-reversed path-pairs that exit the scattering medium with different spatial separations. These time-reversed paths are a direct consequence of Maxwell's equations and represent rays that travel through the same sequence of scattering events, only in the opposite directions of each other. The rays leave the medium with the probability that is specified by the spatially resolved diffuse reflectance profile $I(x,y)$ [see Fig. 1(c)]. The 2D Fourier transform of the spatially resolved intensity distribution defines the angular CBS peak $I(\theta_x,\theta_y)$ [see Fig. 1(d)] as

$$I(\theta_x,\theta_y) = \iint_{-\infty}^{\infty} I(x,y)e^{ik(x\sin\theta_x + y\sin\theta_y)}\mathrm{d}x\mathrm{d}y, \quad (1)$$

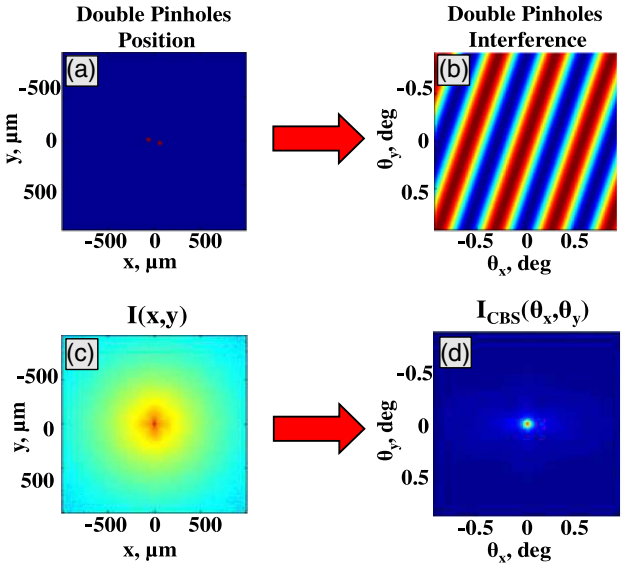

Fig. 1. Schematic presentation of the CBS peak formation. (a) Two pinholes with spatial coordinates. (b) Diffraction pattern from pinholes in terms of angular coordinates. (c) Spatially resolved diffuse reflectance $I(x,y)$. (d) Angular CBS peak defined as the 2D Fourier transform of the spatially resolved intensity distribution $I_{\mathrm{CBS}}(\theta_x,\theta_y) = \mathrm{FT}[I(x,y)]$. See also further details in (Media 1), or see Ref. [10].

where θ_x and θ_y are the angles of backscattering with subscripts x and y indicating the scanning directions.

Akkermans *et al.* [11] derived an equation that governs the shape of the CBS peak using a scalar diffusion approximation:

$$I_{\mathrm{CBS}}(\theta_s) = \frac{3}{8\pi}\left[1 + \frac{2z_o}{l_s^*} + \frac{1}{(1+k\theta_s l_s^*)^2} \cdot \left(1 + \frac{1-\exp(-2k\theta_s z_o)}{k\theta_s l_s^*}\right)\right], \quad (2)$$

where θ_s is the backscattering angle, l_s^* is the transport mean free path, and z_o is the location of the trapping plane (typically assumed as $0.71 l_s^*$).

In the current report, we introduce two major ways of modeling coherent polarized light propagation in scattering tissue-like turbid media with the specific purpose of CBS simulation. We present the current state-of-the-art technique for electric field MC modeling of coherent polarized light propagation in turbid multiple scattering medium and compare two major MC approaches used in simulations of CBS. The first approach is based on tracking the transformations of the electric field along the ray of photon propagation and scattering through the medium, which has been widely implemented by many research groups including Martinez and Maynard [12], Xu [13], Sawicki *et al.* [14], and Radosevich *et al.* [15]. The second approach, pioneered by Kuzmin and Meglinski [16,17], also tracks the electric field along photon trajectories, but it has been developed in analogy to the iterative procedure for the solution of the Bethe–Salpeter equation. We start with a brief introduction of the MC method, and then present, discuss, and compare the results of modeling with the results of the known analytical solution. Finally, the advantages and disadvantages of each technique and their possible further developments are discussed.

2. BASICS OF MONTE CARLO PHOTON MIGRATION MODELING

To the extent of our knowledge, the first implementation of the MC method for simulation of light propagation in biological tissue was introduced by Wilson and Adam in 1983 [18]. Since that time, the MC approach has been further developed [19–25] and widely used for various applications in biomedical optics [26].

The principles behind the conventional MC method are based on modeling energy transfer through the medium, and they have been described comprehensively elsewhere (e.g., [19,25]). Within the practical realization of the approach, a photon packet is first initialized with a weight of one and injected into a modeling semi-infinite medium. Then, the photon packet undergoes a sequence of events representing light-matter (light-tissue) interactions (including scattering, absorption, reflection, and refraction at the medium boundary) until it is either fully absorbed or leaves the medium. The distance (s) that a photon packet propagates between scattering events is determined randomly following the Beer–Lambert law:

$$P(s) = (\mu_a + \mu_s)\cdot \exp(-(\mu_a + \mu_s)s), \quad (3)$$

where μ_a and μ_s are the absorption and scattering coefficients, respectively. After updating the photon packet position, its weight is then reduced by multiplying the current photon weight by the albedo $\mu_s/(\mu_a+\mu_s)$. A new direction of the photon packet is defined at each scattering event by the scattering phase function $F(\theta)$, which is typically described by the Henyey–Greenstein function [27]:

$$F_{\mathrm{HG}}(\theta) = \frac{1}{2}\frac{1-g^2}{(1+g^2-2g\cos\theta)^{3/2}}, \quad (4)$$

where θ is the polar scattering angle ($\theta \in [0,\pi]$) and g is the anisotropy factor, defined as the average $\langle\cos\theta\rangle = \int_{-1}^{1}\cos\theta F_{\mathrm{HG}}(\cos\theta)d\cos\theta$ for any given phase function ($g \in [-1,1]$).

The photon packet continues to travel through the medium according to Eqs. (3) and (4) until it is either fully absorbed or leaves the scattering medium. At this point, any relevant quantities (e.g., the spatial distribution of light exiting the medium) can be recorded. A new photon packet is then initiated, and one follows the same process described above. As soon as a large enough number of photon histories (typically $>10^6$) are tracked to sufficiently reduce numerical uncertainty, the simulation terminates.

Thus, the conventional, or so-called scalar, MC approach does not take into account the wave nature of light, and hence it does not account for associated wave phenomenon such as polarization, coherence, phase retardation, and interference. Nevertheless, the conventional MC method has been widely employed for simulations of fluence rate distributions [21,22,24,25], skin reflectance spectra and color [28–30], and other quantities of interest in biomedical optics [26].

3. CBS ELECTRIC FIELD MONTE CARLO MODEL I

In the scalar MC approach discussed above, the phase and polarization state of each ray are not considered at all. For calculation of CBS, we consider the propagation of time-reversed photon path-pairs. Since these rays travel through

the same path length, the portion of phase change attributable to propagation through space is the same. We, therefore, only consider the changes in phase and polarization due to scattering.

In order to track the phase of the electric field and its changes during propagation in scattering media, MC model I uses the Jones calculus formalism [31]. This algorithm uses a heavily modified version of the Stokes vector meridian plane MC code written by Ramella-Roman *et al.* [5]. Briefly, in the framework of this approach the incident electric field $\mathbf{E}_i$ undergoes three linear transformations to arrive at the scattered electric field $\mathbf{E}_s$ for a single scattering event:

$$\begin{bmatrix} E_{\parallel s} \\ E_{\perp s} \end{bmatrix} = \begin{bmatrix} \cos(\gamma-\pi) & -\sin(\gamma-\pi) \\ \sin(\gamma-\pi) & \cos(\gamma-\pi) \end{bmatrix} \begin{bmatrix} S_2(\theta,\phi) & S_3(\theta,\phi) \\ S_4(\theta,\phi) & S_1(\theta,\phi) \end{bmatrix} \times \begin{bmatrix} \cos\phi & -\sin\phi \\ \sin\phi & \cos\phi \end{bmatrix} \begin{bmatrix} E_{\parallel i} \\ E_{\perp i} \end{bmatrix}, \tag{5}$$

$$\mathbf{E}_s = \mathbf{R}(\gamma-\pi)\mathbf{S}(\theta,\phi)\mathbf{R}(\phi)\mathbf{E}_i, \tag{6}$$

where $\mathbf{R}(\phi)$ is a rotation matrix that transfers the $E_\parallel$ component of the electric field from the initial meridian plane $\mathbf{OP}_1\mathbf{P}_z$ into the scattering plane $\mathbf{OP}_1\mathbf{P}_2$, $\mathbf{S}(\theta,\phi)$ is the amplitude scattering matrix, and $\mathbf{R}(\gamma-\pi)$ transfers $E_\parallel$ back into the meridian plane $\mathbf{OP}_2\mathbf{P}_z$ for further photon propagation. Figure 2 depicts the geometry used in MC model I. Further details describing the use of this geometry in light scattering applications can be found in the seminal works by Chandrasekhar [32] and Kattawar and Plass [1].

The Henyey–Greenstein phase function in Eq. (4) assumes spherically symmetric scattering centers. This assumption removes the ϕ-dependence of function $\mathbf{S}$, as well as the cross-terms $\mathbf{S}_3$ and $\mathbf{S}_4$, leaving

$$\mathbf{S}(\theta) = -ik^3 \cdot F_{\mathrm{HG}}(\theta) \cdot \begin{bmatrix} \cos\theta & 0 \\ 0 & 1 \end{bmatrix}, \tag{7}$$

where k is the wavenumber, $k = 2\pi/\lambda$, and λ is the wavelength of incident light.

In a multiple scattering medium, the single scattering electric field transformations in Eq. (6) accumulate for every scattering event until the photon leaves the medium. Accordingly,

$$\begin{aligned} \mathbf{E}' &= \mathbf{R}_n(-\gamma)\mathbf{S}_n(\theta)\mathbf{R}_n(\phi)\cdots\mathbf{R}_1(-\gamma)\mathbf{S}_1(\theta)\mathbf{R}_1(\phi)\mathbf{E}_i, \\ &= \bar{\mathbf{M}}\mathbf{E}_i, \end{aligned} \tag{8}$$

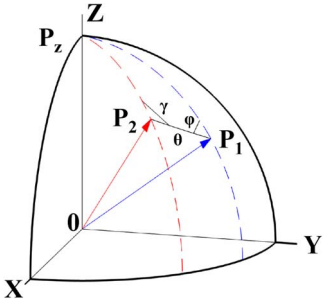

Fig. 2. Geometry of MC model I. For scattering from direction $\mathbf{OP}_1$ to $\mathbf{OP}_2$, three linear transformations of the electric field are made according to Eqs. (5) and (6). ϕ and γ are the angles between the scattering plane and meridian planes $\mathbf{OP}_1\mathbf{P}_z$ and $\mathbf{OP}_2\mathbf{P}_z$, respectively.

where the subscripts $\mathbf{R}$ and $\mathbf{S}$ indicate the number of scattering events, $\mathbf{E}'$ is the electric field leaving the medium after n scattering events, and $\bar{\mathbf{M}}$ represents the effective complex scattering matrix for the entire photon path within the medium.

Thus, in order to calculate the CBS peak the calculation of the effective complex scattering matrix for both the forward ($\bar{\mathbf{M}}_\odot$) and reverse propagating paths ($\bar{\mathbf{M}}_\otimes$) is required. Fortunately, once the forward propagating path has been calculated, the reverse propagating path can be determined easily. For arbitrary complex variables $\tilde{a}$, $\tilde{b}$, $\tilde{c}$, and $\tilde{d}$, the forward propagating path can be succinctly written as

$$\bar{\mathbf{M}}_\odot = \begin{bmatrix} \tilde{a} & \tilde{b} \\ \tilde{c} & \tilde{d}, \end{bmatrix}. \tag{9}$$

The reverse path is then simply [12]

$$\bar{\mathbf{M}}_\otimes = \begin{bmatrix} \tilde{a} & -\tilde{c} \\ -\tilde{b} & \tilde{d} \end{bmatrix}. \tag{10}$$

After the matrices $\bar{\mathbf{M}}_\odot$ and $\bar{\mathbf{M}}_\otimes$ have been calculated, the electric field leaving the scattering sample can be calculated by multiplying the incident electric field $\mathbf{E}$ by the matrix $\bar{\mathbf{M}}$:

$$\mathbf{E}'_\odot = \bar{\mathbf{M}}_\odot\mathbf{E}, \quad \mathbf{E}'_\otimes = \bar{\mathbf{M}}_\otimes\mathbf{E}, \tag{11}$$

where $\mathbf{E}'_\odot$ and $\mathbf{E}'_\otimes$ are the electric fields leaving the medium for the forward and reverse propagating paths, respectively. The incoherent light intensities are then determined for the forward path by calculating the Stokes parameters using $\mathbf{E}'_\odot$ [33]:

$$\begin{aligned} I &= E_\parallel E_\parallel^* + E_\perp E_\perp^*, \\ Q &= E_\parallel E_\parallel^* - E_\perp E_\perp^*, \\ U &= E_\parallel E_\perp^* + E_\perp E_\parallel^*, \\ V &= i(E_\parallel E_\perp^* - E_\perp E_\parallel^*). \end{aligned} \tag{12}$$

Scoring the incoherent intensities according to their exit positions, the spatial distribution of co- ($I_\parallel$) and cross- ($I_\perp$) polarized intensity light exiting the medium can be found as

$$\begin{aligned} I_\parallel(x,y) &= \frac{1}{N_{\mathrm{ph}}}\sum_{i=1}^{N_{\mathrm{ph}}} W_i \cdot [1 + Q(x,y)/I(x,y)], \\ I_\perp(x,y) &= \frac{1}{N_{\mathrm{ph}}}\sum_{i=1}^{N_{\mathrm{ph}}} W_i \cdot [1 - Q(x,y)/I(x,y)], \end{aligned} \tag{13}$$

where W is the photon weight and N_{ph} is the total number of detected photon packets.

In order to determine the extent to which the forward and reverse paths interfere, we define the degree of interference as [15,34]

$$\mathrm{DOI} = \frac{|E_\odot + E_\otimes|^2}{|E_\odot|^2 + |E_\otimes|^2} - 1 = \frac{2\Re[E_\odot E_\otimes^*]}{|E_\odot|^2 + |E_\otimes|^2}, \tag{14}$$

where the symbol $\Re[\cdot]$ indicates the real part of the complex cross-term $E_\odot E_\otimes^*$. DOI takes values between –1 and 1, which represent the total destructive and constructive interference, respectively.

For the linear co-polarized channel, the reciprocity theorem guarantees that each time-reversed path-pair exits the medium with the same accumulated phase. Mathematically, it is seen as an equivalent of the diagonal terms of $\bar{\mathbf{M}}_{\odot}$ and $\bar{\mathbf{M}}_{\otimes}$. As a result, the DOI for the linear co-polarized channel $\mathrm{DOI}_{\parallel}$ is equal to unity. For the linear cross-polarized channel, there is no such guarantee for the phase difference between time-reversed light paths (note that the cross-terms of $\bar{\mathbf{M}}_{\odot}$ and $\bar{\mathbf{M}}_{\otimes}$ are not the same). For a particular photon's trajectory by combining Eqs. (9)–(11), and (14), the DOI for the linear cross-polarized channel $\mathrm{DOI}_{\perp}$ can be found as

$$\mathrm{DOI}_{\perp} = \frac{-2\Re[\tilde{c}\cdot\tilde{b}^{*}]}{|\tilde{c}|^{2}+|\tilde{b}|^{2}}. \tag{15}$$

Thus, the co- ($I_{\parallel}$) and cross- ($I_{\perp}$) polarized intensities of the CBS peak are defined as

$$\begin{aligned} I_{\parallel}(x,y)_{\mathrm{CBS}} &= \frac{1}{N_{\mathrm{ph}}}\sum_{i=1}^{N_{\mathrm{ph}}} W_i\cdot\mathrm{DOI}_{\parallel}\cdot[1+Q(x,y)/I(x,y)],\\ I_{\perp}(x,y)_{\mathrm{CBS}} &= \frac{1}{N_{\mathrm{ph}}}\sum_{i=1}^{N_{\mathrm{ph}}} W_i\cdot\mathrm{DOI}_{\perp}\cdot[1-Q(x,y)/I(x,y)]. \end{aligned} \tag{16}$$

Finally, the angular CBS peak is calculated according to Eq. (1) by taking the 2D Fourier transform of Eq. (16).

4. CBS ELECTRIC FIELD MONTE CARLO MODEL II

The Bethe–Salpeter equation (BSE) [35] describes the transfer of a pair of complex-conjugated fields, incident into the point of source R_S with the wave vector k_i and outgoing in the detecting point R_D with the wave vector k_D. Iterating the BSE presents the intensity of scattered light as the series in scattering orders, where the first term describes single scattering, the second term describes two scattering events, and so forth. Within the MC framework, the scattering intensity can also be presented as the sum of scattering orders [36,37]. Thus, in the second electric field MC algorithm by an analogy to the iterative procedure of the solution of the BSE, polarization tracking in a multiple scattering medium is performed in terms of a polarization vector $\vec{P}$ that undergoes a sequence of transformations after each scattering event. The trajectories of the photon packet are weighted (W) in accordance with the polarization state, and the polarization vector of the scattered wave $\vec{P}_i$ is transformed upon the i-th scattering event as [38]

$$\vec{P}_i = -\vec{e}_i\times[\vec{e}_i\times\vec{P}_{i-1}] = [\hat{I}-\vec{e}_i\otimes\vec{e}_i]\vec{P}_{i-1}, \tag{17}$$

where $\vec{e}_i$ is the unit vector aligned along the trajectory element of a photon packet after the i-th scattering event. Tensor $\hat{\mathbf{S}}_i = [\hat{I}-\vec{e}_i\otimes\vec{e}_i]$ is presented as

$$\hat{\mathbf{S}}_i = \begin{pmatrix} 1-e_{iX}^2 & -e_{iX}e_{iY} & -e_{iX}e_{iZ}\\ -e_{iX}e_{iY} & 1-e_{iY}^2 & -e_{iY}e_{iZ}\\ -e_{iX}e_{iZ} & e_{iX}e_{iZ} & 1-e_{iZ}^2 \end{pmatrix}, \tag{18}$$

and, thus, the chain of projection operators $\hat{\mathbf{S}}_i$ transform the initial polarization $\vec{P}_0$ upon a sequence of n scattering events to the final polarization $\vec{P}_n$, i.e.,:

$$\vec{P}_n = \hat{\mathbf{S}}_n\hat{\mathbf{S}}_{n-1}\ldots\hat{\mathbf{S}}_1\vec{P}_0. \tag{19}$$

Consequently, propagation of co- and cross-polarized components of the electromagnetic field in the medium is described along the same trajectories obtained for the scalar field. The Rayleigh factor is taken into account at every scattering event for the electromagnetic field [38,39] to link the scalar and vector nature of electromagnetic fields according the optical theorem [40,41]:

$$\Gamma = \frac{2}{1+\cos^{2}\theta}. \tag{20}$$

Thus, in the final expression, $I_{\parallel}$ and $I_{\perp}$ are calculated as

$$\begin{aligned} I_{\parallel}(x,y) &= \frac{1}{N_{\mathrm{ph}}}\sum_{i=1}^{N_{\mathrm{ph}}}(W_i P_{x_i}^{2}\Gamma_R^{n_i}\,\exp(-\mu_a L_i)),\\ I_{\perp}(x,y) &= \frac{1}{N_{\mathrm{ph}}}\sum_{i=1}^{N_{\mathrm{ph}}}(W_i P_{y_i}^{2}\Gamma_R^{n_i}\,\exp(-\mu_a L_i)), \end{aligned} \tag{21}$$

where n is the number of scattering events experienced by the i-th photon packet along its trajectory L from the point of incidence R_S to the detector R_D. Respectively, for the CBS peak, the co- and cross-polarized components are [38,39]:

$$\begin{aligned} I_{\parallel}(\theta_x,\theta_y)_{\mathrm{CBS}} &= \frac{1}{N_{\mathrm{ph}}}\sum_{i=1}^{N_{\mathrm{ph}}}(\gamma W_i P_{x_i}^{2}\Gamma_R^{n_i}\,\exp(-\mu_a L_i)) - I_{(1)},\\ I_{\perp}(\theta_x,\theta_y)_{\mathrm{CBS}} &= \frac{1}{N_{\mathrm{ph}}}\sum_{i=1}^{N_{\mathrm{ph}}}(\gamma W_i P_{y_i}^{2}\Gamma_R^{n_i}\,\exp(-\mu_a L_i)), \end{aligned} \tag{22}$$

where $I_{(1)}$ defines the single scattering, γ is the phase factor defined for each photon packet as: $\cos[(k_i+k_D)_{\perp}(R_D-R_S)_{\perp}]\approx\exp(k(x_n-x_i)\theta_s)$, and x defines the angle scanning direction. Finally, the depolarization ratio DR of backscattered light intensity is defined as

$$\mathrm{DR} = \frac{I_{\parallel}-I_{\perp}}{I_{\parallel}+I_{\perp}}. \tag{23}$$

5. RESULTS AND DISCUSSION

We compare the two electric field MC approaches presented above by performing simulations of CBS peaks utilizing the Henyey–Greenstein scattering phase function. Figure 3 shows the results of CBS peak modeling by MC models I and II for different values of anisotropy of scattering (g) and the mean free path length (l_s^{*}). In each simulation, we study the shape of the CBS peak for a scattering mean free path length of 33.3 μm, a representative value within the range of biologically relevant optical properties [42]. For a particular pair of simulations, the R^2 value was calculated as the square of Pearson's linear correlation coefficient between the two MC models [43]. An excellent quantitative agreement has been found between the two electric field MC approaches with

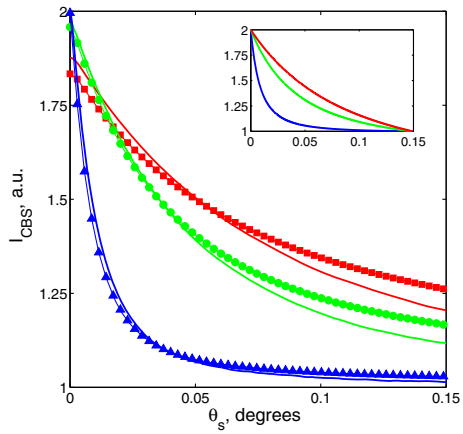

Fig. 3. Angular dependence of CBS for varying anisotropy of scattering. The solid lines indicate the CBS peaks obtained by MC algorithm I. The symbol lines show the results obtained with the MC algorithm II: squares correspond to $g = 0, l_s^* = 33$ μm, circles to $g = 0.5$, $l_s^* = 66.6$ μm, and triangles to $g = 0.9$, $l_s^* = 333.3$ μm. The inset shows results calculated using the scalar diffusion approximation by Akkermans *et al.* [44].

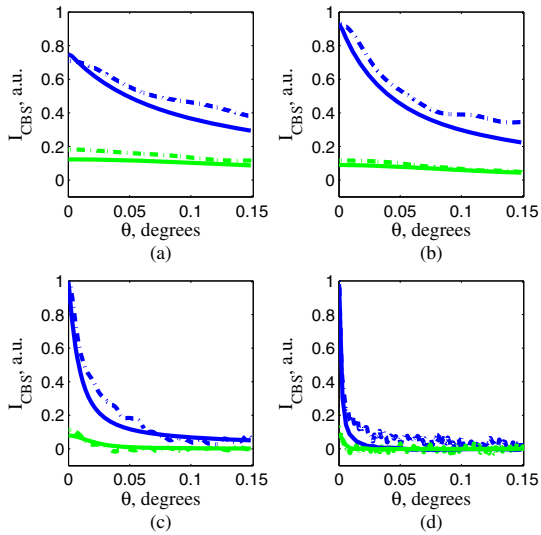

Fig. 4. Angular dependence of co- and cross-polarized CBS components counted for media with different anisotropy of scattering: (a) $g = 0$, (b) $g = 0.5$, (c) $g = 0.9$, and (d) $g = 0.98$. The blue curves represent co-polarized component $I_{CBS}(\theta_x)$, and the green curves show the cross-polarized $I_{CBS}(\theta_y)$ one. The results of simulations obtained by the electric field MC algorithms I and II are presented by solid and dashed lines, respectively.

determination coefficients of $R^2 = 0.97$ for $g = 0$, $R^2 = 0.98$ for $g = 0.5$, and $R^2 = 0.99$ for $g = 0.9$ (see the summarized values in Table 1).

Due to an increase in the anisotropy of scattering ($g \to 1$), there is a corresponding increase in the total photon path length within the medium. As a result of the increased path length, the shape of the CBS peak becomes increasingly more narrow (see Fig. 3). For media with a higher anisotropy of scattering $g \to 1$ (more forward scattering), the height of the CBS peak (h, which is the value of the CBS peak at $\theta_s = 0$) is increased. These changes in the shape of the CBS peak are explained by the fraction of scattering orders that contributed to the constructive and/or destructive interference upon formation of the intensity of CBS [40,44]. This also corresponds to the mathematical interpretation by considering the Fourier transform relationship between the angular peak shape and the spatial separation of light exiting the medium [35].

We also note a good qualitative agreement with the results predicted by Akkerman's diffusion approximation in Eq. (2), as shown in the inset of Fig. 3. It should be pointed out here that the results of simulations shown in Figure 3 are not measurable experimentally since the vector nature of light (i.e., polarization) should be taken into account.

Figure 4 shows the results of CBS peak simulations for linear polarized light. As one can see, the same trends in the CBS peak height and shape, in general, are clearly observed for the same values of anisotropy of scattering (g). While the agreement between the two electric field MC techniques is not as good as in the scalar case (presented in Fig. 3 and Table 1), a high degree of correlation is nevertheless seen in Table 2.

Table 1. Coefficient of Determination between CBS Peaks Counted by the Electric Field MC Algorithms I and II for Media with Different Anisotropy of Scattering

Anisotropy of scattering (g)	0	0.5	0.9
Coefficient of determination (R^2)	0.97	0.98	0.99

Comparing the height of CBS peaks, we noticed that the intensity of the cross-polarized CBS peak is an order of magnitude lower than the intensity of the co-polarized CBS peak. According to the reciprocity theorem, for the co-polarized component each multiply scattered photon path is guaranteed to possess a time-reversed partner and they become fully coherent to each other (i.e., the pairs of photons exit with the same accumulated phase) [34]. Mathematically, this is seen as an equality of the diagonal elements of $\bar{\mathbf{M}}_{\odot}$ and $\bar{\mathbf{M}}_{\otimes}$. In the cross-polarized component, this relationship is not guaranteed and two rays traveling through time-reversed paths may exit with different accumulated phase. This is due to the fact that some of the scattering rotations of photon packets into the cross-polarized configuration are not reversible. In this case, the cross-terms $\bar{\mathbf{M}}_{\odot}$ and $\bar{\mathbf{M}}_{\otimes}$ revealed are not the same. As a result, constructive interference does not appeared for most of the photon packets exiting the medium in frame of the cross-polarized configuration. Thus, the height of the cross-polarized CBS peak becomes much lower than the intensity of the co-polarized CBS peak.

Despite the excellent agreement between MC codes I and II, we acknowledge that minor discrepancies in the shapes of CBS peaks remain (see Fig. 4). In particular, MC code I results in a slightly narrower CBS peak than that of MC code II. This is due to the fact that the implementation of polarization

Table 2. Coefficients of Determination between the Angular Co- (∥) and Cross- (⊥) Polarized Components of the CBS Peak Counted by the Electric Field MC Algorithms I and II for Media with Different Anisotropy of Scattering (g)

g	0	0.5	0.9	0.98
$R^2_{\parallel}$	0.63	0.82	0.90	0.60
$R^2_{\perp}$	0.52	0.72	0.82	0.66

tracking is based on different theoretical concepts between the two codes. The MC code I uses a semi-analytical modeling approach that very accurately takes into account the low scattering orders. In contrast, MC code II operates by full photon trajectories and requires more photon statistics to obtain the CBS peaks with the shapes identical to those obtained by MC code I.

Figure 5 shows the spatial distributions of the co- ($I_{\parallel}(x,y)$) and cross- ($I_{\perp}(x,y)$) polarized intensities of backscattered light detected on the medium surface. We note that there is an excellent qualitative agreement between the results of simulations obtained by both electric field MC models. An equally good agreement between the results has also been obtained for media with different scattering anisotropy ($g = 0, 0.5, 0.98$; results are not presented here for brevity).

If the polarization of incident light and detection of polarization are oriented along the x-axis, a lesser amount of light scatters in the direction orthogonal to the initial polarization resulting in an elongation of the spatial distribution of $I_{\parallel}(x,y)$. For $I_{\perp}$, a cross pattern is formed since the cross-polarized component of the phase function is primarily oriented along these directions (i.e., 45°, 135°, 225°, and 315°).

Modeling of a large number of photon packet trajectories (typically 10^{11}) can be extremely resource consuming, and this was a significant concern in the MC models developed in the past [29]. Both models have been implemented utilizing the advantages of parallel programming on NVIDIA Graphics Processing Units (GPUs) using Compute Unified Device Architecture (CUDA). The particular details of GPU implementation for simulation of coherent polarized light propagation in turbid tissue-like scattering medium are described in [45]. Performance of both models has been tested and compared utilizing stand-alone Tesla M2090/Tesla K20X parallel processors.

For the MC model I, which is based on tracking transformations of the electric field along the ray propagation, the time required to simulate 10^6 photon packet trajectories is dependent on the parameters of the scattering medium and source-detector configuration. For instance, computing the CBS peak for a semi-infinite scattering medium ($l_s = 33.3$ μm, $g = 0.9$, and $\mu_a = 0.0001$ mm^{-1}) takes ≈30 s. For the MC model II, a simulation using the same medium parameters takes ≈15 s to compute, i.e., nearly in realtime.

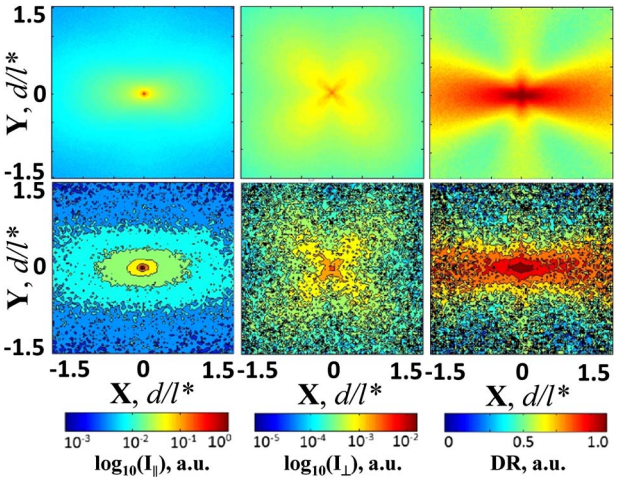

Fig. 5. Spatial distributions of backscattered light $I_{\parallel}(x,y)$, $I_{\perp}(x,y)$, and DR(x,y) at the surface of the medium obtained by electric field MC algorithms I (top row) and II (bottom row). Both simulations were performed for semi-infinite scattering medium ($l_s = 33.3$ μm, $g = 0.9$, $\mu_a = 0.001$ mm^{-1}) with the normal incidence of light. 10^9 photon packets have been tracked in each simulation.

A NVIDIA visual profiler was used to perform automated analysis of the codes with the aim of identifying bottlenecks and obtaining optimization suggestions that can be used to improve the overall performance of MC models. Both models demonstrate the extensive use of GPU global memory. However, the negative effects were almost eliminated by the GDDR5's bandwidth (up to 177 GB/s). Furthermore, CUDA multiprocessor occupancy has been accessed. The multiprocessor occupancy is the ratio between the actual number of threads running in parallel and the maximum number of threads in which resources can be stored on-chip simultaneously (known as the maximum occupancy) [45]. Maximizing occupancy helps hide the effects of long latency accesses during global memory loads and therefore can improve the bandwidth-bound program's performance. For model I, the occupancy was ≈37%, and model II demonstrated a value of ≈63%. Thus, both codes have the potential for further optimization.

The open-source code for model I is available on the website of the Biophotonics Laboratory at Northwestern University (http://biophotonics.bme.northwestern.edu/resources). For practical use as well as for further validation and possible further developments, the electric field MC modeling of photon migration in scattering tissue-like media is now available for the immediate use online as part of the browser-based MC modeling tool at www.biophotonics.ac.nz [29].

6. SUMMARY AND CONCLUSIONS

The results of two electric field MC modeling approaches developed independently for simulation of CBS have been compared. Good agreement was found for the scalar ($R^2 > 0.97$) and vector cases (R^2 between 0.52 and 0.9). In order to be more fully relevant to the scenarios present for actual tissue measurements, the comparison between these electric field MC models will be extended to include the effects of reflection/refraction at the medium boundary, circular polarization, and different phase functions based on Mie theory. Current and further developments include the integration of the developed MC models of CBS simulation into an online GPU MC modeling environment using peer-to-peer computing infrastructure.

ACKNOWLEDGMENTS

A. Doronin and I. Meglinski acknowledge partial support provided by the Health Research Council of New Zealand (HRC) and the Maurice Wilkins Centre (MWC). A. J. Radosevich was supported by a National Science Foundation Graduate Research Fellowship under Grant No. DGE-0824162.

REFERENCES

1. G. W. Kattawar and G. N. Plass, "Radiance and polarization of multiple scattered light from haze and clouds," Appl. Opt. **7**, 1519–1527 (1968).
2. S. Bartel and A. Hielscher, "Monte Carlo simulations of the diffuse backscattering Mueller matrix for highly scattering media," Appl. Opt. **39**, 1580–1588 (2000).

3. X. Wang and L. Wang, "Propagation of polarized light in birefringent turbid media: a Monte Carlo study," J. Biomed. Opt. **7**, 279–290 (2002).
4. D. Cote and A. Vitkin, "Robust concentration determination of optically active molecules in turbid media with validated three-dimensional polarization sensitive Monte Carlo calculations," Opt. Express **13**, 148–163 (2005).
5. J. Ramella-Roman, S. Prahl, and S. Jacques, "Three Monte Carlo programs of polarized light transport into scattering media: Part I," Opt. Express **13**, 4420–4438 (2005).
6. Y. Kuga and A. Ishimaru, "Retroreflectance from a dense distribution of spherical particles," J. Opt. Soc. Am. A **1**, 831–835 (1984).
7. L. Tsang and A. Ishimaru, "Backscattering enhancement of random discrete scatterers," J. Opt. Soc. Am. A **1**, 836–839 (1984).
8. P. E. Wolf and G. Maret, "Weak localization and coherent backscattering of photons in disordered media," Phys. Rev. Lett. **55**, 2696–2699 (1985).
9. M. P. V. Albada and A. Lagendijk, "Observation of weak localization of light in a random medium," Phys. Rev. Lett. **55**, 2692–2695 (1985).
10. The media file representing the enhancement of CBS is also available on-line at: www.biophotonics.ac.nz/Media/BioTube.aspx.
11. E. Akkermans, P. Wolf, R. Maynard, and G. Maret, "Theoretical study of the coherent backscattering of light by disordered media," J. Phys. **49**, 77–98 (1988).
12. A. S. Martinez and R. Maynard, "Faraday effect and multiple scattering of light," Phys. Rev. B **50**, 3714–3732 (1994).
13. M. Xu, "Electric field Monte Carlo simulation of polarized light propagation in turbid media," Opt. Express **12**, 6530–6539 (2004).
14. J. Sawicki, N. Kastor, and M. Xu, "Electric field Monte Carlo simulation of coherent backscattering of polarized light by a turbid medium containing mie scatterers," Opt. Express **16**, 5728–5738 (2008).
15. A. J. Radosevich, J. D. Rogers, L. R. Apolu, N. N. Mutyal, P. Pradhan, and V. Backman, "Open source software for electric field Monte Carlo simulation of coherent backscattering in biological media containing birefringence," J. Biomed. Opt. **17**, 115001 (2012).
16. V. L. Kuzmin and I. V. Meglinski, "Coherent multiple scattering effects and Monte Carlo method," JETP Lett. **79**, 109–112 (2004).
17. I. Meglinski, V. Kuzmin, D. Churmakov, and D. Greenhalgh, "Monte Carlo simulation of coherent effects in multiple scattering," Proc. Roy. Soc. Lond. Ser. A **461**, 43–53 (2005).
18. B. Wilson and G. Adam, "A Monte Carlo model for the absorption and flux distributions of light in tissue," Med. Phys. **10**, 824–830 (1983).
19. S. A. Prahl, M. Keijzer, S. L. Jacques, and A. J. Welch, "A Monte Carlo model of light propagation in tissue," Proc. SPIE **IS5**, 102–111 (1989).
20. S. Flock, M. Patterson, B. Wilson, and D. Wyman, "Monte Carlo modeling of light propagation in highly scattering tissue-I: model predictions and comparison with diffusion theory," IEEE Trans. Biomed. Eng. **36**, 1162–1168 (1989).
21. M. Keijzer, S. Jacques, S. Prahl, and A. Welch, "Light distributions in artery tissue: Monte Carlo simulations for finite-diameter laser beams," Lasers Surg. Med. **9**, 148–154 (1989).
22. I. V. Yaroslavsky and V. V. Tuchin, "Light penetration through multilayered turbid media: a Monte Carlo simulation," Opt. Spectrosc. **72**, 134–139 (1992).
23. R. Graaff, A. Dassel, M. Koelink, F. de Mul, J. Aarnoudse, and W. Zijlstra, "Condensed Monte Carlo simulations for the description of light transport," Appl. Opt. **32**, 426–434 (1993).
24. L. Wang, S. Jacques, and L. Zheng, "MCML—Monte Carlo modeling of light transport in multi-layered tissues," Comput. Methods Programs Biomed. **47**, 131–146 (1995).
25. S. L. Jacques and L. V. Wang, "Monte Carlo modeling of light transport in tissues," in *Optical Thermal Response of Laser Irradiated Tissue*, A. J. Welch and M. J. C. van Gemert, eds. (Plenum, 1995), pp. 73–100.
26. C. Zhu and Q. Liu, "Review of Monte Carlo modeling of light transport in tissues," J. Biomed. Opt. **18**, 050902 (2013).
27. L. Henyey and J. Greenstein, "Diffuse radiation in the galaxy," Astrophys. J. **93**, 70–83 (1941).
28. I. Meglinski, "Modeling the reflectance spectra of the optical radiation for random inhomogeneous multi-layered highly scattering and absorbing media by the Monte Carlo technique," Quantum Electron. **31**, 1101–1107 (2001).
29. A. Doronin and I. Meglinski, "Online object oriented Monte Carlo computational tool for the needs of biomedical optics," Biomed. Opt. Express **2**, 2461–2469 (2011).
30. G. I. Petrov, A. Doronin, H. T. Whelan, I. Meglinski, and V. V. Yakovlev, "Human tissue colour as viewed in high dynamic range optical spectral transmission measurements," Biomed. Opt. Express **3**, 2154–2161 (2012).
31. R. C. Jones, "A new calculus for the treatment of optical systems," J. Opt. Soc. Am. **31**, 488–493 (1941).
32. S. Chandrasekhar, *Radiative Transfer* (Courier Dover Publications, 1960).
33. C. F. Bohren and D. R. Huffman, *Absorption and Scattering of Light by Small Particles* (Wiley, 1983).
34. R. Lenke and G. Maret, "Multiple scattering of light: Coherent backscattering and transmission," in *Scattering in Polymeric and Colloidal Systems* (Gordon and Breach, 2000), pp. 1–73.
35. M. Rossum and T. Nieuwenhuizen, "Multiple scattering of classical waves: microscopy, mesoscopy, and diffusion," Rev. Mod. Phys. **71**, 313–371 (1999).
36. M. Y. Kirillin, I. V. Meglinski, and A. V. Priezzhev, "Effect of photons of different scattering orders on the formation of a signal in optical low-coherence tomography of highly scattering media," Quantum Electron. **36**, 247–252 (2006).
37. E. Berrocal, D. L. Sedarsky, M. E. Paciaroni, I. V. Meglinski, and M. A. Linne, "Imaging through the turbid scattering media Part II: spatial and temporal analysis of individual scattering orders via Monte Carlo simulation," Opt. Express **15**, 10649–10665 (2007).
38. V. Kuzmin and I. Meglinski, "Numerical simulation of coherent back-scattering and temporal intensity correlations in random media (overview)," Quantum Electron. **36**, 990–1002 (2006).
39. V. L. Kuzmin and I. Meglinski, "Coherent effects of multiple scattering for scalar and electromagnetic fields: Monte Carlo simulation and Milne-like solutions," Opt. Commun. **273**, 307–310 (2007).
40. E. Akkermans and G. Montambaux, *Mesoscopic Physics of Electrons and Photons* (Cambridge University, 2011).
41. P. S. Carney, E. Wolf, and G. S. Agarwal, "Statistical generalizations of the optical cross-section theorem with application to inverse scatter," J. Opt. Soc. Am. A **14**, 3366–3371 (1997).
42. V. V. Tuchin, *Tissue Optics: Light Scattering Methods and Instruments for Medical Diagnosis*, 2nd ed. (SPIE, 2007).
43. M. G. Kendall and A. Stuart, *The Advanced Theory of Statistics* (Hafner, 1961), Vols. 2 and 3.
44. E. Akkermans, P. E. Wolf, and R. Maynard, "Coherent backscattering of light by disordered media: analysis of the peak line shape," Phys. Rev. Lett. **56**, 1471–1474 (1986).
45. A. Doronin, C. Macdonald, and I. Meglinski, "Propagation of coherent polarized light in turbid highly scattering medium," J. Biomed. Opt. **19**, 025005 (2014).